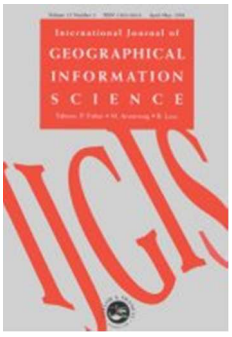

Characterization of active fault scarps from LiDAR data: a case study from Central Apennines (Italy)

Journal:	*International Journal of Geographical Information Science*
Manuscript ID:	IJGIS-2011-0452.R3
Manuscript Type:	Special Issue Paper
Keywords:	Terrain analysis < Keywords Relating to Theory, Geomorphology < Keywords Relating to Application, Geological mapping and modelling < Keywords Relating to Application

Characterization of active fault scarps from LiDAR data: a case study from Central Apennines (Italy)

CARLO ALBERTO BRUNORI, RICCARDO CIVICO, FRANCESCA ROMANA CINTI, GUIDO VENTURA*
Istituto Nazionale di Geofisica e Vulcanologia, 00143 Roma, Italy

*Corresponding author: Guido Ventura - Istituto Nazionale di Geofisica e Vulcanologia, Via di Vigna Murata 605, 00143, Roma, Italy Phone: (+39) 0651860221 E-mail: guido.ventura@ingv.it

Abstract. A high resolution DEM (1 ms spacing) derived from an airborne LiDAR campaign was used in an attempt to characterize the structural and erosive elements of the geometry of the Pettino fault, a seismogenic normal fault in Central Apennines (Italy). Four 90- to 280 m -long fault scarp segments were selected and the surface between the base and the top of the scarps was analyzed through the statistical analysis of the following DEM-derived parameters: altitude, height of the fault scarp, distance along strike, slope and aspect. The results identify slopes of up to 40° in faults lower reaches interpreted as fresh faces, 34° up the faces. The Pettino fault maximum long slipe-rate (0.6-1.1 mm/yr) was estimated from the scarp heights, which are up to 12 and 19 m in the selected four segments, and the age (ca. 18 ka) of the last glacial erosional phase in the area. The combined analysis of the DEM-derived parameters allow us to (a) define aspects of 3D scarp geometry, (b) decipher its geomorphological significance, and (c) estimate the long-term slip rate.

Keywords: LiDAR; Fault scarp; Morphology; Pettino fault (Abruzzi)

1. Introduction

High-resolution topographic data such as LiDAR (Light Detection and Ranging)-derived digital elevation models (DEMs) allow us to qualitatively and quantitatively analyze landscapes resulting from tectonic, hillslope, fluvial, biologic and anthropogenic activity. Earth-science

applications of LiDAR include coastal change studies (e.g., Sallenger *et al*. 1999), monitoring of landslides (e.g., Dietrich *et al*. 2001; Glenn *et al*. 2006; Ventura *et al.* 2011), measurement of volcanic deformation (e.g., Hasegawa *et al*. 2007), identification of faults (e.g., Haugerud *et al*. 2003; Sherrod *et al*. 2004; Cunningham *et al*. 2006; Kondo *et al*. 2008; Arrowsmith and Zielke, 2009), and estimates of slip-rate (e.g., Frankel *et al*. 2007). In the last decade, there have been several studies on the geometry of fault scarps using high-resolution LiDAR data (e.g., Chan *et al.* 2007; Begg and Mouslopoulou, 2010; De Long *et al*. 2010; Hilley *et al*. 2010; Amos *et al*. 2011). However, investigations on the spatial distribution of slope and aspect on active fault scarps, as well as the statistical analysis of these scarp parameters, are still lacking. To partly fill this gap, we extract slope and aspect values from an airborne LiDAR-derived DEM on selected fault scarps of a major, seismogenic fault located in central Apennines (Italy). This study examines the fault scarp morphology of the active Pettino fault (central Apennines, Italy) and identifies the effects of tectonic and erosion processes on the scarp face through the statistical and spatial analysis of high resolution (1x1 m pixel) aspect and slope morphometric parameters. The method allowed the quantification of the fault morphology (e.g., scarp heights, slope of fresh and degraded scarps). The paper is organized as follows: at first, we provide a basic review and conceptualization of the time evolution of fault scarps; in a second step, we describe the Pettino fault in the geological framework of the study area ; in the third step we illustrate the LiDAR data elaboration procedure, and quantify the fault morphology through slope and aspect from LiDAR DEM. The statistical analysis of these parameters allow us to detail the fault geometry and the processes recognition.

2. Morphology of fault scarps

Scarps characterize most of dip to oblique-slip faults. Fault-scarp terminology is derived from observations made on piedmont scarps (Wallace, 1977; Bull, 2007). The general evolution of

a fault scarp and the principal morphologic features of a scarp are summarized in the sketch of Fig. 1, where the construction of an idealized scarp by repeated slip is shown, along with the effects of possible degradation and aggradation processes. The base of the scarp and the crest are the lower and upper extremes of a fault scarp, respectively and the scarp height is measured as the vertical separation between them. The free-face is the fresh exposed surface resulting from slip on a fault. A fault scarp, once it is formed, immediately start to degrade (e.g., Stewart and Hancock, 1990). The free-face retreats upslope and colluvial materials begin to accumulate at the base of the scarp, forming a debris slope. Renewed slip episodes on a pre-existing fault scarp may abruptly steepen the slope producing a characteristic segmented appearance of the topographic profile with a rounded crest and a steep free-face.

3. Geological setting of the Pettino fault

The Pettino fault is located in the L'Aquila town region within the central Apennines, a well-known seismically prone area. Here, the NE-verging fold-and-thrust mountain belt from Neogene compressive tectonics is dissected by an intense NE-SW striking extension that, since Late Pliocene and Quaternary times, has led to the formation of intermountain basins controlled by NW-SE striking faults (e.g., Doglioni, 1995; Cipollari and Cosentino, 1995; Ghisetti and Vezzani, 1999) (Fig. 2). Historical earthquakes larger than M≥5.5 mostly occurred on these NW-SE striking faults, which are characterized by normal to oblique-slip, and are up to 15-20 km long. These faults extend in depth to 10–15 km with dip 50°-70°, mostly SW-side down (Lavecchia *et al*. 1994; Vezzani and Ghisetti, 1998; Barchi *et al*. 2000; Galadini and Galli, 2000; Foglio CARG 2009). Pre-existing, NNE-SSW and ESE-WNW to NW-SE, low-angle (dip <45°) contractional structures also outcrop (Pizzi and Galadini, 2009) and, in many cases, their geometry influences the extensional tectonics, with reactivation of pre-existing structures (Ghisetti and Vezzani, 2002; Patacca *et al*. 2008; Di

Luzio *et al*. 2009; Di Luccio *et al*. 2010). One of the normal faults bordering the northern side of the Aterno river, i.e., the Paganica fault, ruptured to the surface during the April 2009 L'Aquila sequence (e.g. Emergeo Working Group, 2010).

The main geological units of the area can be summarized as follows. Jurassic-Miocene limestones and marls, and Miocene sandstones represent the bedrock outcropping on the ridges and valley flanks. Quaternary deposits include Pleistocene breccias, lacustrine and alluvial deposits (Blumetti *et al*. 2002). Local debris alluvial fans occur at the foot of the valley.

We focus our analysis on the Pettino fault, a part of the Late Quaternary segmented system called the Upper Aterno fault system (e.g. Blumetti, 1995, 1997), which is responsible for the evolution of the L'Aquila basin, and likely, for the 1703 A.D., M>6 earthquake (Fig. 2; Galadini and Galli, 2000). We selected the Pettino fault because the associated scarps appear, at a field survey scale, quite continuous and homogeneous along the trace; the scarps do not cut large urban areas for most of their length, even if local modifications induced by anthropic activities occur.

The ca. 10 km long, 100°-120°-striking, 60° SW dipping Pettino fault emerges NW of the L'Aquila city center along the slope of the carbonatic Pettino ridge and marks the boundary between the hills dipping towards the southwest and Late Pleistocene sediments. As most of the faults in the Apennines, the limestone fault scarp is exposed, and a zone of cataclasite is in tectonic contact against the stratified slope deposits. Detailed structural measurements, i.e. strike and dip of fault plane at different locations on the Pettino fault are, however, not reported in the literature. As concerns the height of the fault scarp, Galli *et al.* (2011) report an average height of 10 m in one outcrop along the southern portion of the fault. At the NW termination of the Mt. Pettino Fault an alluvial terrace is vertically displaced 15-20 m (Galadini and Galli, 2000). Based on this offset a vertical slip rate of 0.47-0.86 mm/yr since upper Pleistocene is assigned to the whole Upper Aterno fault system (Galadini *et al*. 2001).

4. LiDAR data and analytical methods

The LiDAR measures and collects multiple returns of a laser beam aimed at the ground and is able to discriminate between the first return, usually from the top of the forest canopy, and the last return, from the bare earth surface. By isolating the last returns, LiDAR is capable of revealing the ground surface even in highly vegetated areas. The airborne LiDAR survey of the study area was performed and processed a few days after the 6 April 2009 L'Aquila earthquake by the Civil Protection of Friuli Venezia Giulia (Italy) using an Optech ALTM 3100 EA Airborne Laser Terrain Mapper System. The main technical parameters related to the LiDAR acquisition and errors are listed in Table 1. Vertical errors (1σ) are less than 0.2 m and horizontal errors less than 0.54 m.

We create a regular 1 by 1 m DEM from the LiDAR bare-earth point cloud by means of the inverse distance weighted interpolation method with a 3 m search radius using the routine IDW of ArcInfo by ESRI. Within the constructed DEM, we selected a 2.8 km x 2.1 km area including the central portion of the Pettino fault (Figs. 2 and 3). The shaded relief, slope and aspect digital maps derived from the DEM of the Pettino area were used to identify fault scarps as described below. Slope and aspect were calculated using a 3 x 3 m moving window, which is the minimum window size to determine these parameters, following Moore *et al.* (1993).

Airphotographs, high spatial resolution satellite images, and DEMs were used in order to interpret fault scarps and manmade features (roads, walls, quarries). Analytical steps of the fault surface extraction are: 1) computation of slope and aspect; 2) identification of the base and top of morphological scarps from shaded relief images, slope, and aspect maps; in particular, we extract the limits of the the scarp surface based on abrupt changes in topography and slope (Fig. 4); 3) fault scarps were discriminated from manmade features by the aid of IKONOS panchromatic images with 1 m spatial resolution and QUICKBIRD with a 0.6 m resolution; 4) definition of an area for

each fault scarp bounded by the base and the top of the scarp as defined in point 2 above and depicted in Fig. 4. Identification of the limits of the scarp surfaces is mainly based on slope changes and experience in the field. Numerical criteria have not been developed for scarp identification because of the presence of incisions and large aspect variations of the surface, and so are not used here.

Based on the procedure described above, four fault scarp segments (hereafter S1, S2, S3 and S4 from SE to NW) have been selected among the Pettino traces (Figs. 3 and 4). Identified limits of the fault, namely lines along their top and base, are termed 'reference lines', and these comprise 1 m spaced digitized 'reference points'. The 'origin' of a fault's area is the westerly extremity of its basal reference line. The final dataset contains, for each point of the selected scarps, the following parameters: absolute position (lat, long), absolute altitude, distance in meters from origin of buffered area (map-view distance of nearest reference point from the fault's origin), relative elevation (highest altitude minus minimum altitude within the fault scarp), down-dip slope (degrees) and aspect (azimuth of down-dip direction from North).

The values of relative elevation from the nearest reference point permit the measurement of fault scarp dimensions (vertical and horizontal) and allow a quantitative comparison between geometries of the different selected scarps. The number of points in each fault scarp are: 3139 (S1), 6512 (S2), 5511 (S3) and 2152 (S4).

5. Results

The results of the selected dataset relative to the fault scarps S1, S2, S3 and S4 are summarized in Figs. 4 to 9. Figures 4 and 5 show the 3D view of the fault scarps and the elevation (in m) of the scarps along the fault strike. Fig. 6 summarizes the statistics (median, lower and upper quartile, variation range) of the altitude, slope and aspect in the selected fault scarps. Figure 5

shows that the scarps have the maximum height (crest to base) between 12.2 and 19.6 m, the average height is 13.4 m with a standard deviation of 2.9, the minimum height is 2 m. The northern tip of S1 has the same elevation of the southern tip of S2, as well as S3 and S4, whereas a break in elevation of about 3 m occurs between S2 and S3. Therefore, a lateral continuity in the elevation characterizes S1 and S2, and S3 and S4. It is worth noting that the break in elevation occurs between the scarps S2 and S3 that are arranged in a left step. This step is also evidenced by the different altitude (m a.s.l.) of S2 and S3 (Fig. 6). The median value, the interquartile distance and the variation range of slope decrease from S1 to S4, whereas the median value of aspect increases (Fig. 6). The preferred values in an aspect-slope, density contour projection (Fig. 7) of the S1-S4 DEM, also indicate a general decrease of slope (from 40° to 34°) from S1 to S4, and an increase of aspect (from 223° to 236°). The spatial variation of slope and aspect values along the scarps (Fig. 8) shows that these values are not homogenously distributed within the scarps. In detail, the higher values of slope mainly occur in the middle and lower part of the scarps, in particular in S1 and S2. The distribution of the aspect values indicate along strike variations, with sub-vertical bands of nearly constant values not equally spaced along the strike. Elevation vs. slope and aspect diagrams (Fig. 9) evidence that, in S1, S3 and S4, the higher slope values (35°-45°) concentrate in the lower part of the scarps at elevation < 4-5 m from the base; at elevations > 4-5 m, the slope values generally decrease (25°-35°). The aspect shows more complex distributions with an increase in the dispersion of values as the elevation increases.

6. Discussion and conclusions

The collected data and results indicate that the Pettino scarps are transversally eroded by drainage which locally produces gullies evidenced by minima in elevation in Fig. 5. On average, the maximum elevation values are located in S2. The average height of the scarp is about 3 m larger

than that measured in an outcrop located about 500 m south of S1 (Blumetti, 1995, 1997; Galli *et al*. 2011). We measure the scarp height using our LiDAR data at the same location of Galli *et al.* (2011) along 2 to 5 m spaced sub-parallel profiles oriented perpendicularly to the fault trace and obtain a value of 10±1 m. This value is fully consistent with that measured by Galli *et al.* (2011). We hypothesize that the fault scarp height slightly decreases southward. However, this hypothesis must be supported by other type of data (e.g. detailed topographic leveling) because of the artificial modification of the Pettino scarp south of S1.

The measured 3 m difference in scarp height between the southeastern tip of S3 and the northwestern tip of S2 is associated with a 110 m wide, 75 m high left step scarp. The southeastern tip of S3, which is 12 m high, reaches the 15 m of overall cumulative deformation adding the about 3 m high scarps parallel to S3 located along the northwestern prolongation of the S2 segment (Fig. 3). Therefore, the left step between S2 and S3 has the significance of a fault overlap, lacking evidence of step-over traces. This has implications in the evaluation of the near field faulting hazard since the deformation during a slip event may be distributed on different, sub-parallel segments. Moreover, the detailed knowledge of the amount of scarp heights, representing the cumulative deformation from multi-slip events, is the base for long term estimates of the slip rate along faults. The maximum 12 to 19 m high Pettino fault scarp (Fig. 5) formed after the erosive phase of the last glaciation (ca. 18 ka; Dramis, 1983; Giraudi and Frezzotti, 1997). Therefore, we calculate a long-term slip rate of the Pettino fault between 0.6 and 1.1 mm/yr. This range of values is congruent with the upper Pleistocene-present 0.47-0.86 mm/yr values of the Upper Aterno fault system (Galadini *et al*. 2001).

The distribution of slope in S1, S3 and S4 (Figs. 8 and 9) records an increase in dip (from less than 35° to 45°, on average) in the lowest 4-5 m of the scarps. Such a higher sloped zone may represent a fresh fault scarp (see Fig. 1) associated with recent faulting event(s). We remark that this

zone does not identify the free-face of the last event being the dip assigned to the Pettino fault plane 60° (Galli *et al.,* 2011). The about 10 m high, upper slope zone has the morphology of an older, degraded scarp. The above described fault scarp morphological features are consistent with those observed in the field on other normal active faults of the Abruzzi region, where the slope values are always less than the subsurface fault dip (e.g., Pantosti *et al.* 1996). Our type of analysis of slope on active faults may give a quantitative constraint to the interpretation of scarps. When considering the distribution of aspect on the Pettino scarps (Figs. 6 and 9), we note that the S4 aspect values concentrate in a more restricted range with respect to those of S1 to S3. This datum indicates that the S4 surface has a lower 'rugosity'. This could be the result of less concentrated erosion processes, associated with a poorly mature surface drainage on S4 (Fig. 3). This conclusion is supported by the lack of significant stream incisions in the area of S4 and by the presence of mature streams in S1-S3 (Fig. 3).

Fig. 7 shows a decrease of slope and an increase of aspect from S1 to S4. This reflects a progressive change in the fault scarp geometry over a length of 1.8 km (Fig. 3). This implies that surface faulting features may show a structural variability over short distances. In the Pettino case, assuming that the maximum value of aspect in Fig. 7 is orthogonal to the fault strike, the strike changes from N133°E to N146°E, i.e. 13° on 1.8 km. The maximum values of slope, which change from 40° (S1) to 34° (S4), could be associated with the changes in strike, thus reflecting a gentle flatting of the fault dip.

In summary, the results of the morphometric analysis on the Pettino fault scarps using airborne LiDAR-derived data highlight the efficacy of our approach in (a) the spatial characterization of scarps, (b) the definition of fault scarp complexity, and (c) understanding the relation among surface ruptures, fault geometry and behavior, and exogenous processes.

Acknowledgments

The LiDAR data was provided by Civil Protection of Friuli Venezia Giulia (Italy). We thank the four IJGIS reviewers George Hilley, George Miliaresis and two anonymous for useful comments, and Carlos H. Grohmann for the editorial handling. Thanks also to A. Smith for the revision of text. Contributions: C.B. elaborated the LiDAR DEM and extracted the slope and aspect maps, R.C. reviewed the available LiDAR literature and constructed figure 1, F.C. and G.V. had the idea to use LiDAR data in fault characterization, provided the spatial statistical analyses, and wrote most of the paper.

References

CINTI, F.R., PANTOSTI, D., DE MARTINI, P.M. PUCCI, S., CIVICO, R., PIERDOMINICI, S., CUCCI, L., BRUNORI, C.A., PINZI, S. AND PATERA, A., 2011, Evidence for surface faulting events along the Paganica fault prior to the 6 April 2009 L'Aquila earthquake central Italy. *Journal of Geophysical Research*, **116**, B07308, doi:10.1029/2010JB007988.

AMOS, C.B., KELSON, K.I., ROOD, D.H., SIMPSON, D.T., ROSE, .S. 2010, Late Quaternary slip rate on the Kern Canyon Fault at Soda Spring, Tulare County, California. *Lithosphere*, **26**, pp. 411-417.

ARROWSMITH, J.R. and ZIELKE, O., 2009, Tectonic geomorphology of the San Andreas Fault zone from high resolution topography: An example from the Cholame segment. *Geomorphology*, doi:10.1016/j.geomorph.2009.01.002.

BARCHI, M., GALADINI, F., LAVECCHIA, G., MESSINA, P., MICHETTI, A.M., PERUZZA, L., PIZZI, A. and TONDI, E. 2000, Sintesi delle conoscenze sulle faglie attive in Italia Centrale: parametrizzazione ai fini della caratterizzazione della pericolosita` sismica. *Gruppo Nazionale per la Difesa di terremoti*, pp. 1-62.

BEGG, J.G. and MOUSLOPOULOU, V., 2010, Analysis of late Holocene faulting within an active rift using lidar, Taupo Rift, New Zealand. *Journal of Volcanology and Geothermal Research*, **190**, pp. 152–167.

BLUMETTI, A.M., BAGNAIA, R., FERRELI, L., GIULIANI, R., MATTONE, M., MICHETTI, A.M., SARVUCCI, R. and VITTORI, E., 1997, Fagliazione superfi ciale e tettonica quaternaria nell'alta Valle dell'Aterno. Abstract at Congress "Tettonica quaternaria del territorio italiano: conoscenze, problemi ed applicazioni", Parma, 25-27 February 1997.

BLUMETTI, A. M., 1995, Neotectonic investigation and evidence of paleosesmicity in the epicentral area of the January-February 1703, central Italy, earthquake. *In*: L. Serva and D. B. Slemmons eds. *Perspectives in paleoseismology*, Association of Engineering Geologists Special Publication, **6**, 83-100.

BLUMETTI, A. M., DI FILIPPO, M., ZAFFIRO, P., MARSAN, P. and TORO B., 2002, Seismic hazard of the city of L'Aquila Abruzzo-central Italy: New data from geological, morphotectonic and gravity prospecting analysis, *Studi Geologici Camerti*, **1**, pp. 7–18.

BULL, W.B., 2007, *Tectonic Geomorphology of Mountains: A New Approach to Paleoseismology*. Wiley-Blackwell, London.

CHAN, Y.C., CHEN, Y.G., SHIH, T.Y. and HUANG, C., 2007, Characterizing the Hsincheng active fault in northern Taiwan using airborne lidar data; detailed geomorphic features and their structural implications, *Journal of Asian Earth Sciences,* **31.3**, pp. 303-316.

CIPOLLARI, P., and COSENTINO, D., 1995., Miocene unconformities in the Central Apennines: geodynamic significance and sedimentary basin evolution. *Tectonophysics*, **252**, pp. 375–389.

CUNNINGHAM, D., GREBBY, S., TANSEY, K., GOSAR, A., and KASTELIC, V., 2006, Application of airborne LiDAR to mapping seismogenic faults in forested mountainous terrain, southeastern Alps, Slovenia. *Geophysical research Letters,* **33**, L20308, doi:10.1029/2006GL027014.

DeLong, S.B., Hilley, G.E., Rymer, M.J.. and Prentice, C., 2010, Fault zone structure from topography: Signatures of en echelon fault slip at Mustang Ridge on the San Andreas Fault, Monterey County, California. *Tectonics*, **29**, TC5003, doi: 10.1029/2010TC002673.

Di Luccio, F., Ventura, G., Di Giovambattista, R., Piscini, A., and Cinti. F. R. 2010, Normal faults and thrusts re-activated by deep fluids: the 6 April 2009 Mw 6.3 L'Aquila earthquake, central Italy. *Journal of Geophysical Research*, **115**, B06315,doi:10.1029/2009JB007190

Di Luzio, E., Mele, G., Tiberti, M.M., Cavinato, G.P. and Parotto, M., 2009, Moho deepening and shallow upper crustal delamination beneath the central Apennines. *Earth Planetary Science Letters*, **280**, pp. 1–12.

Dietrich, W.E., Bellugi, D. and Asua, R.R., 2001, Validation of the Shallow Landslide Model, SHALSTAB, for Forest Management. *In: Land Use and Watershed: Human Influence on Hydrology and Geomorphology in Urban Forest Areas*. *Water Science Application AGU*, **2**, pp. 195-227.

Doglioni, C. 1995, Geological remarks on the relationships between extension and convergent geodynamic settings. *Tectonophysics,* **252**, pp. 253–267.

Dramis, F., 1983, Morfogenesi di versante nel Pleistocene superiore in Italia: I depositi detritici stratificati. *Geografia Fisica Dinamica Quaternaria*, **6**, pp. 180–182.

EMERGEO Working Group, 2010, Evidence for surface rupture associated with the Mw 6.3 L'Aquila earthquake sequence of April 2009 central Italy. *Terra Nova*, **22**, pp. 43–51,

Foglio CARG 1:50,000, 2009, *Cartografia Geologica Ufficiale*. Foglio CARG 359 L'Aquila.

Frankel, K.L., Dolan, J. F., Finkel, R. C., Owen, L. A. and Hoeft, J. S., 2007, Spatial variations in slip rate along the Death Valley-Fish Lake Valley fault system determined from LiDAR topographic data and cosmogenic ^{10}Be geochronology. *Geophysical Research Letters,* **34**, L18303, doi:10.1029/2007GL030549.

GALADINI, F. AND GALLI, P., 2000, Active tectonics in the Central Apennines Italy-input data for Seismic Hazard Assessment. *Natural Hazards*, **22**, pp. 225–270.

GALADINI, F., MELETTI, C. and VITTORI, E., 2001, Major active faults in Italy: available surficial data, Netherlands. *Journal of Geosciences,* **80,** pp. 273-296.

GALLI, P., GIACCIO, B., MESSINA, P., PERONACE, E. and ZUPPI, G.M., 2011, Palaeoseismology of the L'Aquila faults central Italy, 2009, Mw 6.3 earthquake: implications for active fault linkage. *Geophysical Journal International*, doi 10.1111/j.1365-246X.2011.05233.x

GHISETTI, F. AND VEZZANI, L., 1999, Depth and modes of Pliocene–Pleistocene crustal extension of the Apennines Italy. *Terra Nova*, **11**, pp. 67–72.

GHISETTI, F. and VEZZANI L., 2002, Normal faulting, transcrustal permeability and seismogenesis in the Apennines Italy. *Tectonophysics*, **348**, pp. 155–168.

GIRAUDI, C. and FREZZOTTI, M., 1997, Late Pleistocene glacial events in the central Apennines, Italy. *Quaternary Research,* **48**, pp. 280–290.

GLENN, N.F., STREUTKER, D.R., CHADWICK, D.J., THACKRAY, G.D. and DORSCH, S.J. 2006, Analysis of LiDAR-derived topographic information for characterizing and differentiating landslide morphology and activity. *Geomorphology*, **73**, pp. 131-148.

HASEGAWA, H., SATO, H.P. and IWAHASHI J., 2007, Continuous Caldera Changes in Miyakejima Volcano after 2001. *Bulletin of Geospatial Information Authority of Japan*, **54**, pp. 60-64.

HAUGERUD, R.A., HARDING, D.J., JOHNSON, S.Y., HARLESS, J., WEAVER, C.S., and SHERROD, B.L. 2003, High-resolution lidar topography of the Puget Lowland, Washington - A bonanza for earth science. *GSA Today*, **13**, pp. 4–10.

HILLEY, G.E., DELONG, S., PRENTICE, C., BLISNIUK, K. and ARROWSMITH, J.R., 2010, Morphologic dating of fault scarps using airborne laser swath mapping ALSM data. *Geophysical Research Letters,* **37**, L04301, doi:10.1029/2009GL042044.

KONDO, H., TODA, S., OKUMURA, K., TAKADA, K. and CHIBA, T., 2008, A fault scarp in an urban area identified by LiDAR survey: A Case study on the Itoigawa–Shizuoka Tectonic Line, central Japan. *Geomorphology,* **101**, pp. 731-739.

LAVECCHIA, G., BROZZETTI, F., BARCHI, M., MENICHETTI, M. AND KELLER, J.V.A., 1994, Seismotectonic zoning in east-central Italy deduced from an analysis of the Neogene to present deformations and related stress fields. *Geological Society of America Bulletin*; **106**, pp. 1107-1120

MOORE, I. D., LEWIS, A. GALLANT J. C., 1993, Terrain properties: Estimation Methods and Scale Effects, Modeling Change in Environmental Systems. In A.J. Jakeman et al. editors, John Wiley and Sons, New York.

PANTOSTI, D., G. D'ADDEZIO, AND CINTI F.R., 1996, Paleoseismicity of the Ovindoli-Pezza fault, central Apennines, Italy: a history including a large, previously unrecorded earthquake in Middle Ages (860-1300 A.D.). *Journal of Geophysical Research*, 101, No. B3, 5937-5959,.

PATACCA, E., SCANDONE, P., DI LUZIO, E., CAVINATO, G., and PAROTTO, M., 2008, Structural architecture of the central Apennines: Interpretation of the CROP 11 seismic profile from the Adriatic coast to the orographic divide. *Tectonics*, **27**, TC3006, doi:10.1029/2005TC001917.

PIZZI, A., and GALADINI, F., 2009, Pre-existing cross-structures and active fault segmentation in the northern-central Apennines Italy. *Tectonophysics*, **476**, pp. 304–319

SALLENGER, A.H., KRABILL, W., BROCK, J., SWIFT, R., JANSEN, M., MANIZADE, S., RICHMOND, B., HAMPTON, M., and ESLINGER, D., 1999, Airborne laser study quantifies El Niño-induced coastal change. *Eos Transactions American Geophysical Union*, **80**, pp. 92–93.

SHERROD, B.L., BROCHER, T.M., WEAVER, C.S., BUCKNAM, R.C., BLAKELY, R.J., KELSEY, H.M., NELSON, A.R. and HAUGERUD, R., 2004, Holocene fault scarps near Tacoma, Washington, USA. *Geology,* **32**, pp. 9-12.

STEWART, I.S. and HANCOCK, P.L., 1990, What is a fault scarp? *Episodes*, **13**, pp. 256–263.

VENTURA, G., VILARDO, G., TERRANOVA, C., BELLUCCI SESSA, E., 2011, Tracking and evolution of complex active landslides by multi-temporal airborne LiDAR data: The Montaguto landslide (Southern Italy). *Remote Sensing of Environment,* **115**, pp. 3237-3248, doi:10.1016/j.rse.2011.07.007

VEZZANI, L. AND GHISETTI, F., 1998, Carta Geologica dell_Abruzzo, Scala 1:100,000. *SELCA*, Firenze.

WALLACE, R.E., 1977, Profiles and ages of young fault scarps, north-central Nevada. *Geological Society of America Bulletin,* **88**, pp. 1267-1281.

Figure captions

Figure 1. a) Sketch illustrating an idealized composite fault scarp profile and its time evolution. b) Different view of a composite fault scarp.

Figure 2. Structural schematic map of the L'Aquila town region (Central Apennines, Italy) with major faults and historical earthquakes epicenters. The faults located between L'Aquila and Montereale towns belong to the Upper Aterno fault system. Quaternary basins include Pleistocene breccias and lacustrine deposits. The remnant areas are Jurassic to Miocene limestones and marls, and Miocene sandstones. The dashed rectangle includes the study area shown in Fig. 3. Modified from Cinti e *et al*. (2011) and references therein.

Figure 3. Shaded relief from LiDAR data of the area including the central sector of the Pettino fault (see Fig. 2). Red lines (numbered from S1 to S4) are the base of the fault scarps selected for this study. Black lines are the base of the fault scarps mapped but not included in our analysis.

Figure 4. 3D view of the selected S1 to S4 Pettino fault scarps (location in Fig. 3). The S1 to S4 bottom and crest are delineated with shaded lines, which delimit the buffer area on which the aspect and slope have been estimated; the elevation and distance along strike parameters are also shown.

Figure 5. Distance along strike vs. elevation of the S1 to S4 Pettino fault scarps. The elevation is calculated from the base of the scarp upward.

Figure 6. Box-plot diagrams summarizing the statistics of altitude (m a.s.l.), slope (°) and aspect (°) parameters from LiDAR-derived DEM in the S1 to S4 scarps.

Figure 7. Circular plots of the density contours (in %) of the distribution of slope and aspect values (calculated from DEM) of pixels belonging to the S1 to S4 scarps.

Figure 8. Distribution of the slope (to the left) and aspect (to the right) values on the S1 to S4 scarp surface calculated from DEM.

Figure 9. Elevation vs. slope (up) and aspect (down) pseudo-circular plots for S1 to S4 scarps from DEM-extracted data. Each point represents a pixel.

Table 1. Summary of the LiDAR acquisition parameters.

System	Optech ALTM 3100 EA
Operating altitude	80 – 3500 m
Vertical accuracy	10 cm < 1000 m (1 σ) 15 cm < 2000 m (1 σ) 20 cm <3000 m (1 σ)
Horizontal accuracy	1/5500 x flying altitude (1 σ)
Range resolution	1 cm
Scan angle	Variable from 0 to ± 25°
Swath width	Variable from 0 m to 0.93 x altitude
Angular resolution	0.01°
Scan frequency	Variable, maximum 70 Hz
Laser wavelength	1064 nm
Laser repetition rate	Variable from 33 to 100 kHz
Beam divergence	Variable: 0.2 mrad (1/e) or 0.8 mrad (1/e)
"Eye safe" altitude limit	80 m - 0.8 mrad 400 m - 0.2 mrad
Intensity	Measurement of intensity of each pulse received
Collected data	Simultaneous measurement in range of first and last pulse for each pulse emitted
Laser classification	Class IV laser products (FDA CFR 21)
GPS receiver	Internal Novatel Millennium DL
Power requirements	28 VDC @35 A peak
Operating temperature	15-35 °C
Humidity	0-95 % non-condensing

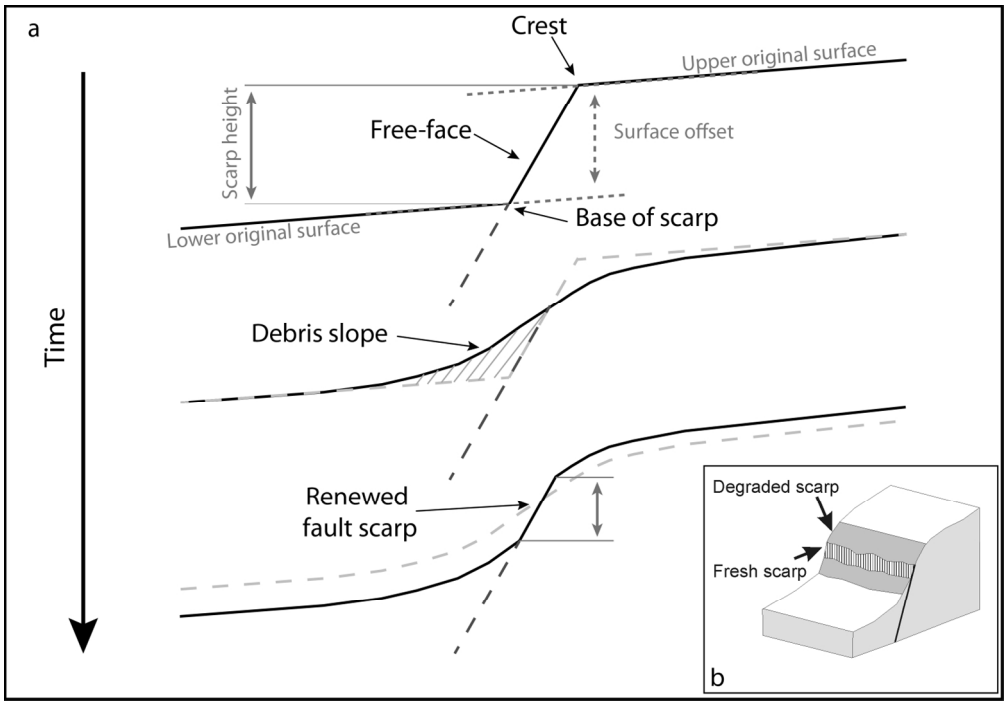

Figure 1. a) Sketch illustrating an idealized composite fault scarp profile and its time evolution. b) Different view of a composite fault scarp (simplified from Stewart and Hancock, 1990).
133x92mm (300 x 300 DPI)

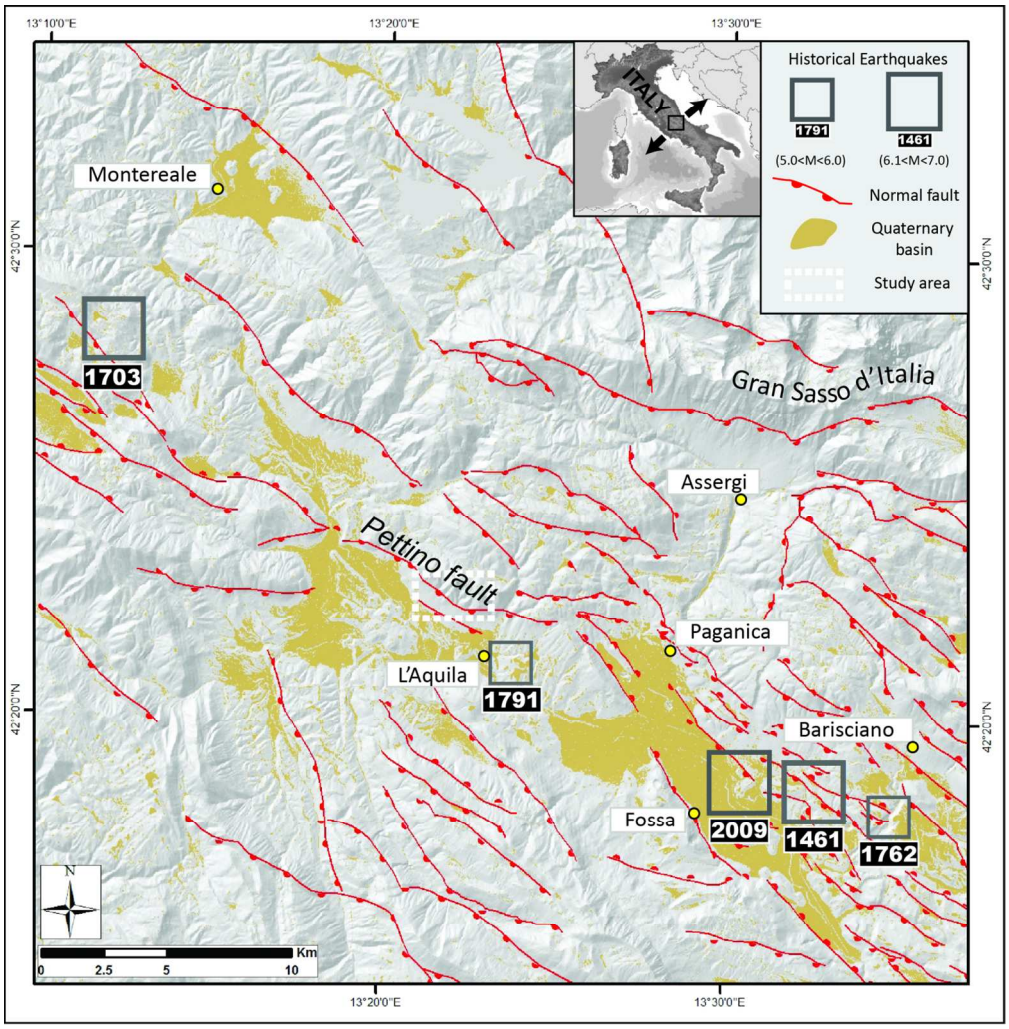

135x137mm (300 x 300 DPI)

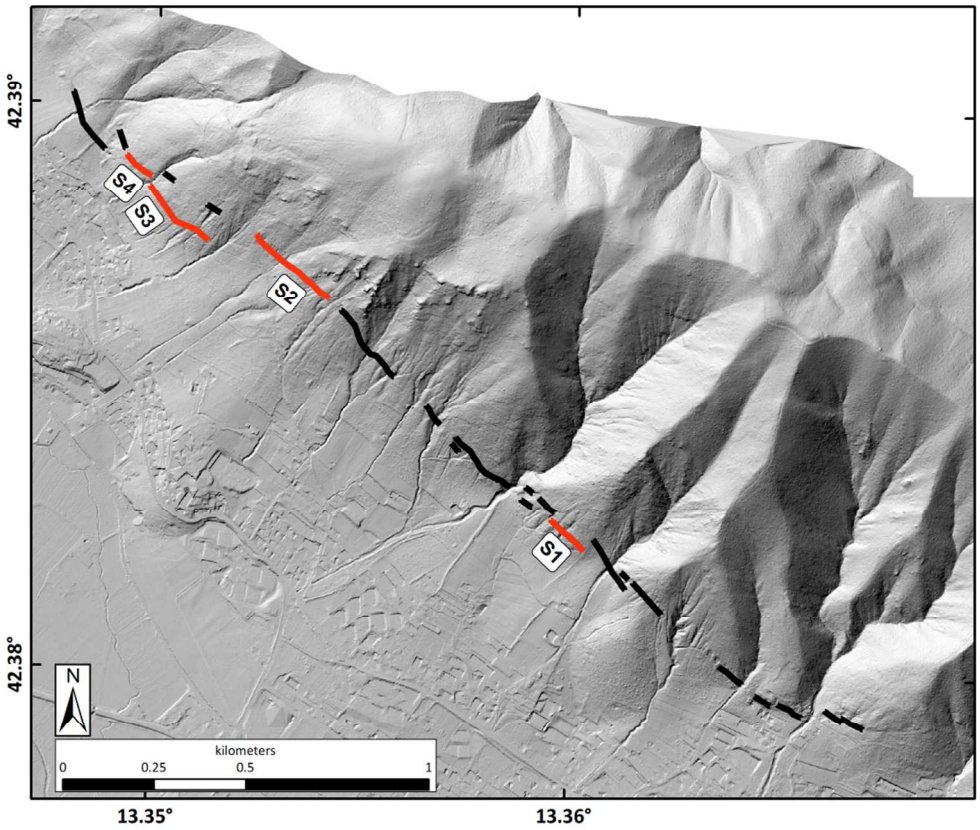

99x84mm (300 x 300 DPI)

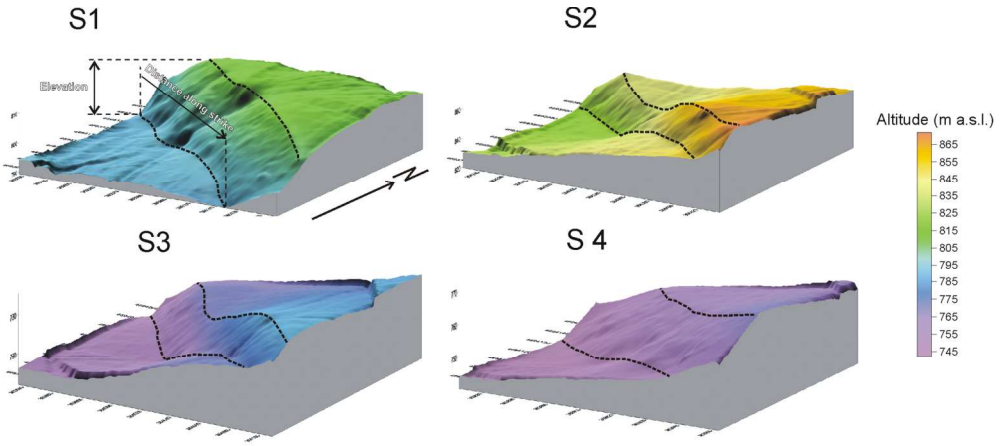

157x68mm (300 x 300 DPI)

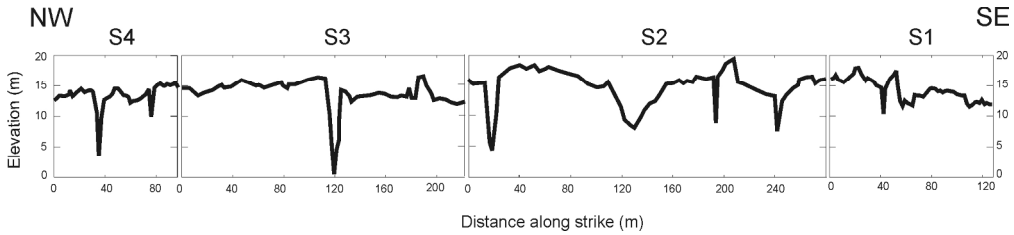

200x44mm (300 x 300 DPI)

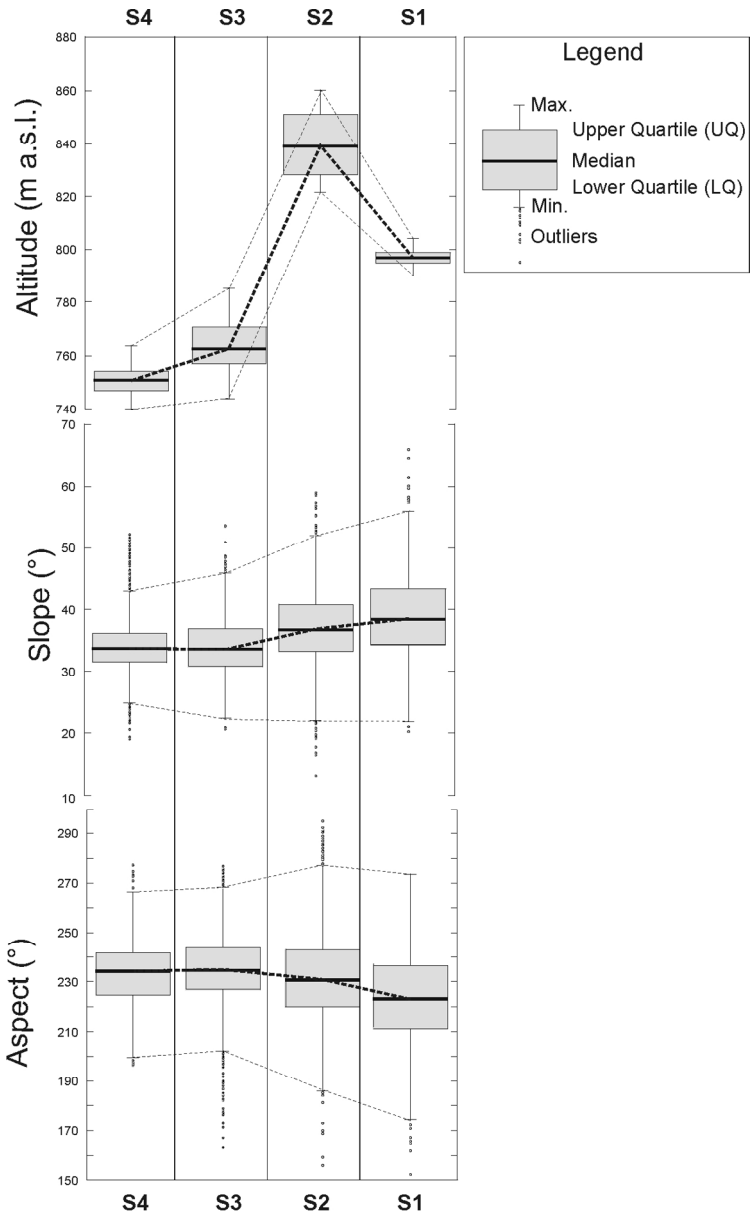

107x174mm (300 x 300 DPI)

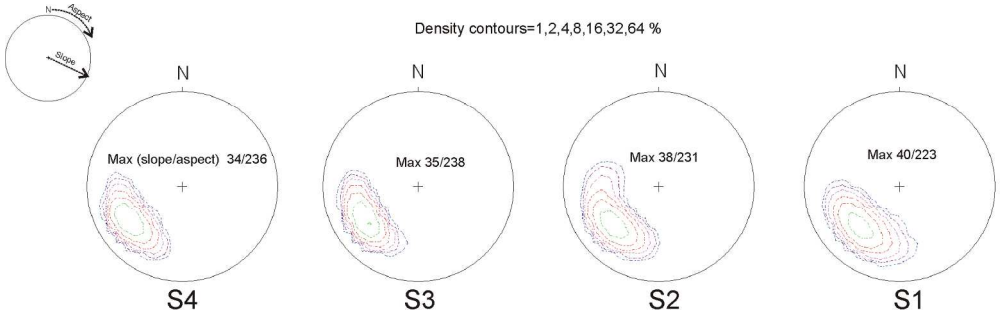

187x57mm (300 x 300 DPI)

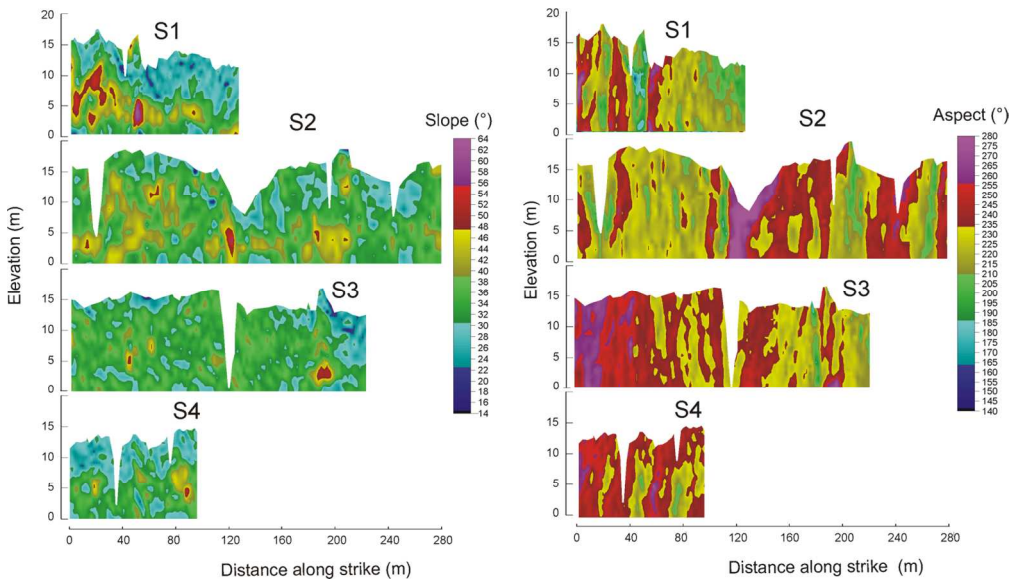

137x79mm (300 x 300 DPI)